PHYSICAL REVIEW D **90,** 105015 (2014)

Instanton bags, high density holographic QCD, and chiral symmetry restoration

S. Bolognesi*

Department of Physics Enrico Fermi and INFN, University of Pisa, Largo Pontecorvo, 3, Ed. C, 56127 Pisa, Italy
and Department of Mathematical Sciences, Durham University, Durham DH1 3LE, United Kingdom

(Received 16 June 2014; published 11 November 2014)

We describe the simplest example of an instanton bag in Euclidean space. It consists of a monopole wall and a Kaluza-Klein monopole wall, lifted to one higher dimension, trapping the instanton charge in the middle. This object has finite instanton density in a three-dimensional volume. Baryon physics in holographic QCD models gets translated into a multi-instanton problem in the bulk, and a state with a high density baryonic charge consists of a nondiluted multi-instanton solution. The instanton bag is a good candidate for this high-density state. We compute its parameters via moduli stabilization. Chiral symmetry restoration is exhibited by this state, and it is a direct consequence of its nondiluted features.

DOI: 10.1103/PhysRevD.90.105015 PACS numbers: 21.65.Qr, 11.25.Tq, 11.27.+d, 12.38.Aw

I. INTRODUCTION

Holographic QCD (HQCD) has been the subject of intense studies because it provides an environment to address strong coupling QCD questions with the use of semiclassical computations. Baryons of the QCD-like theory defined on the boundary correspond to instantons in the bulk. Thus, having a finite baryonic density in the dual theory corresponds to having a finite density of instantons in the bulk. The problem of the high-density phase of QCD is thus translated into a multi-instanton problem, which, even at the classical level, remains quite a difficult challenge, both numerically and analytically. Recently with Sutcliffe, we considered a toy model in $2+1$ dimensions in which the high-density phase can be studied both analytically and numerically [1]. This model showed that the dilute approximation breaks down, as expected, exactly at the densities when the solitons are sufficiently close to start to populate the holographic direction.

Solitons are not hard objects but can compenetrate with one another. A high-density phase of solitons may be in the form of a collective structure, which is completely different from a coarse-grained version of a large number of small constituents. This phenomenon has been observed both for vortices and monopoles [2] and is known as the "solitonic bag." We still do not have a proper soliton bag description for multi-instanton configurations, although it has been suggested that this should somehow exist [3,4]. One obstacle in finding such a solution for instantons is that for the Yang-Mills theory in Euclidean space, instantons do not have an intrinsic scale. Thus, it is not uniquely defined how to make a high-density limit of instantons; the sizes must be specified in the limiting process. HQCD is a situation in which instantons do have an intrinsic scale. This scale is fixed by a balance between the curvature of the background geometry and the Chern-Simons coupling, which makes the instanton electrically charged. We may expect that a large number of instantons in HQCD could form a bag structure at large enough density.

QCD at high density is expected to exhibit a phase transition in which chiral symmetry is restored. Moreover, there is a competition between two other possible instabilities: color superconductivity and chiral density waves. The second one is favored in the large N_c limit [5,6]. Holographic models of QCD, being particular cases of large N_c QCD-type models, are thus expected to have chiral symmetry restoration together with chiral waves. Recently, these questions have been addressed in HQCD [7], where it has been found that, using an instanton fluid approximation, there is no sign of those phases. We will show that they are instead realized in the instanton bag background. Another generic expectation from large N_c QCD is the existence of a "quarkyonic phase" [8]. This is generally believed to correspond, in HQCD, to the instantons populating the holographic direction [7,9,10], so that many instantons share the same 3D spatial section. Yet a different phase in HQCD has been discussed in [11,12] and named "dyonic salt." This phase is analogue to the half-Skyrmion phase in the high-density Skyrme model and, for this reason, it has been argued to exhibit chiral symmetry restoration. The instanton bag we discuss in the present paper can be considered as an extension of the dyonic salt phase to densities where the instantons start to populate the holographic direction. In a sense, this paper is a reconciliation of various approaches. Our state is also similar to the almost homogeneous state considered in [13], but with a different motivated ansatz.

The paper is organized as follows. In Sec. II we describe an instanton bag solution in flat space. In Sec. III we review

*stefanobolo@gmail.com

some generic features of HQCD at finite density. In Sec. IV we embed the instanton bag in HQCD and study the moduli stabilization. In Sec. V we review the top-down derivation of the Sakai-Sugimoto model. In Sec. VI we discuss the phenomenon of chiral symmetry restoration at large densities. We conclude in Sec. VII.

II. AN INSTANTON BAG FROM MONOPOLE WALLS

We consider a Yang-Mills (YM) theory in 5D Minkowski space-time with gauge group $SU(2)$. The action is

$$S_{YM5} = -\int dt d^4x \frac{1}{4g^2} F^a_{\mu\nu} F^{\mu\nu a}. \tag{2.1}$$

Instantons correspond to particles with mass $8\pi^2/g^2$. We will consider solutions that are periodic in one direction, and thus we can formally compactify the x_3 direction on a circle of radius R_3 (we chose the direction 3 for later convenience). The sector of configurations that are also invariant along x_3 have the 4D Yang-Mills-Higgs (YMH) action

$$S_{YMH4} = -\int dt dx_1 dx_2 dx_4 \frac{\pi R_3}{2g^2} (F^a_{\mu\nu} F^{\mu\nu a} + D_\mu \phi^a D^\mu \phi^a), \tag{2.2}$$

where ϕ is just another name for A_3. This is the first term in a Kaluza-Klein (KK) series expansion. The monopole wall studied in [14,15] (see also [16–21]) is a solution of the Bogomol'nyi equations $F_{ij} = \epsilon_{ijk} D_k \phi$ for the YMH action (2.1) and thus, lifted to 4D by keeping the fields x_3 independent, it is also a self-dual instanton solution satisfying $F = \tilde{F}$.

A sketch of the monopole wall solution is given in Fig. 1. The wall is located at a fixed position in x_4 and is extended in the $x_{1,2,3}$ directions. The wall separates two phases, one on the left in which A_3 is constant and the field strength is vanishing, and the other on the right in which A_3 grows linearly with x_4 and the magnetic B field is constant. This is in the singular gauge in which the fields far from the wall are directed in a fixed direction in the su(2) algebra, and Dirac string singularities are on the empty left side of the wall. The Bogomol'nyi equation $B = F_{34}$ implies that A_3 is growing linearly as a function of x_4. Details about the non-Abelian nature and its lattice structure are all contained in a small strip near the wall and can be neglected at large distances. When this solution is lifted to 4D, the monopoles become monopole strings extended in the x_3 direction and the wall becomes a three-dimensional object.

The monopole wall solution is specified by the following set of parameters. The first is the area of the unit monopole lattice in the 1–2 plane. We name l the typical distance between the constituents' monopoles and l^2 is the area of the unit lattice in the 1–2 plane. The magnetic field sourced by the wall is then related to the microscopic structure by

$$F_{12} = B t_{\mathrm{su}(2)} \qquad B = \frac{4\pi}{l^2}, \tag{2.3}$$

which is obtained by requiring that one unit of magnetic flux pass through each cell. Also, $t_{\mathrm{su}(2)}$ is any normalized generator of $SU(2)$; for example, $t_3 = \mathrm{diag}(1/2, -1/2)$. In this singular gauge, the field F_{12} is constant far from the wall. The field A_3 is then given by

$$A_3|_{x_3<0} = 0 \quad \text{and} \quad A_3|_{x_3>0} = B x_3 t_{\mathrm{su}}(2). \tag{2.4}$$

The transverse thickness of the wall is of order

$$\delta \simeq \frac{1}{\sqrt{B}}, \tag{2.5}$$

being the scale where massive W bosons start to condense near the wall. As long as we are interested in length scales much greater than the lattice size l and the transverse thickness δ, the microscopic details of the monopole wall are not relevant. The monopole wall solution has a constant

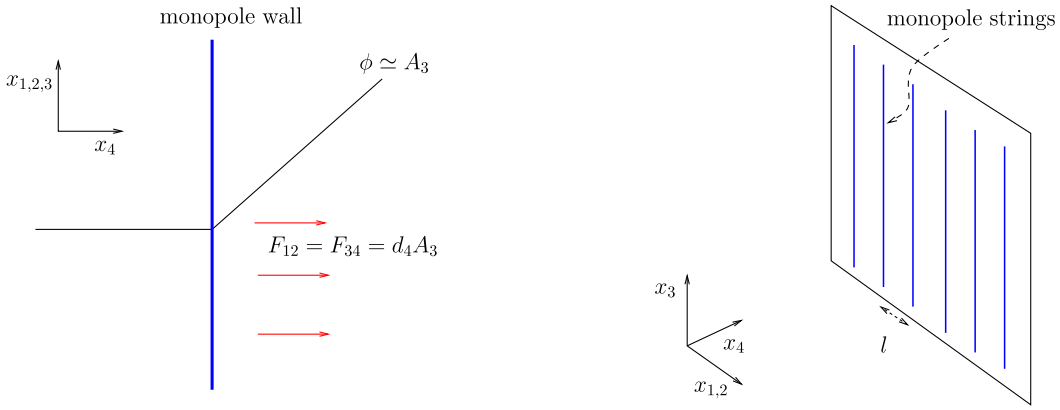

FIG. 1 (color online). Monopole wall.

instanton charge and also constant energy density on the right side and zero on the left side.

The monopole wall, at the microscopic level, necessarily breaks translational invariance. This is somehow analogue to the nonexistence of exactly spherical symmetry monopoles for charge higher than 1 [22]. The lattice structure of the monopole wall has been studied in some detail using numerical techniques in [15] for the BPS case and in [17] for AdS_4 where the hexagonal lattice has been found to be slightly favored energetically. For the present paper, we do not need to know the details of the lattice structure because we consider only the large scale properties.

A monopole wall in isolation is not enough to have finite instanton density in $\mathbb{R}^3$. For this, we also need a wall of Kaluza-Klein (KK) monopoles, or a "KK monopole wall." KK monopoles are solutions of YM equations on $\mathbb{R}^3 \times S^1$ with a nontrivial dependence on the compactified direction. They carry the same instanton charge of the monopole but an opposite magnetic charge. One instanton on $\mathbb{R}^3 \times S^1$ is then decomposable into one monopole plus one KK monopole [23–25], and the distance between the constituents is continuously connected with the scale modulus of the instanton. We will show that with a monopole wall and a KK monopole wall, we can create a configuration that has finite instanton density in a three-dimensional volume.

When the theory is compactified on a circle S^1, so with the periodic identification $x_3 \equiv x_3 + 2\pi R_3$, we can make a gauge transformation that is topologically distinct from the identity map

$$U(x_3) = e^{-ix_3 t_{\mathrm{su}(2)}/R_3}. \tag{2.6}$$

This function interpolates between the identity matrix with plus and minus sign as x_3 completes its period. If the theory contains only adjoint fields, the gauge transformation (2.6) connecting the two elements of the center of the group 1 and -1 is thus single valued. This gauge transformation shifts the gauge field by a constant

$$A_3 \to A_3 - \frac{t_{\mathrm{su}(2)}}{R_3}. \tag{2.7}$$

Therefore, the gauge field A_3 assumes value in a T-dual circle.

The KK monopole is an ordinary monopole transformed by a large-gauge transformation action plus a global gauge transformation that flips the sign of the generator $t_{\mathrm{su}(2)} \to -t_{\mathrm{su}(2)}$. The KK monopole has opposite sign relation between the instanton charge and the monopole charge. For example if we normalize so that the monopole has $(n_{\mathrm{mon}}, n_{\mathrm{inst}})$ charge equal to $(1/2, 1/2)$, the KK monopole has charges $(-1/2, 1/2)$. So the monopole together with a KK monopole has exactly the charge of an instanton (0,1). The asymptotic value of the Higgs field is $\phi \equiv A_3 \simeq t_{\mathrm{su}(2)}/2R_3$, so the large-gauge transformation (2.7) plus the global transformation leave it invariant, and the monopole and KK monopole can be glued together. The global transformation flips the sign of both $d_r A_3$ and the magnetic field so that it does not affect the instanton charge.

The KK monopole wall can be obtained in a similar fashion by applying two transformations to the monopole wall. First we use the same large-gauge transformation (2.6) and then a π rotation in the x_3, x_4 plane: $x_{3,4} \to -x_{3,4}$ and $x_{1,2} \to x_{1,2}$. Gauge fields are vectors, so A_3 flips sign with this rotation. On the initial left side of the wall, the empty half $x_4 < 0$, the composition of the two transformations gives the following:

$$A_3 = 0 \to -\frac{t_{\mathrm{su}(2)}}{R_3} \to +\frac{t_{\mathrm{su}(2)}}{R_3}. \tag{2.8}$$

Moreover, the empty side is moved to the right side of the wall $x_4 > 0$. On the nonempty side, the one filled with magnetic field $x_4 > 0$, the field F_{12} remains unchanged because $x_{1,2}$ are not affected by the rotation. Also $d_4 A_3$ is unchanged because both d_4 and A_3 flip the sign. Therefore, both the monopole wall and KK monopole wall satisfy the BPS equation with the same sign. The transformation we have described is exactly what we need to glue together the two walls. The two transformations are shown in Fig. 2.

A monopole wall together with a KK monopole wall is capable of trapping the instanton charge in the middle of the two plates in the x_4 direction. They can be glued together since the B field and the derivative of A_3 have the same sign (see Fig. 3). The microscopic scales are the lattice size l and the transverse thickness δ. The distance between the two walls is d. A_3 grows linearly between the two walls from 0 to $1/R_3$. The BPS equation gives the following relation:

$$B = \frac{1}{dR_3}. \tag{2.9}$$

The instanton charge is still infinite in the directions $x_{1,2,3}$, but it is finite if interpreted as a density in the unit of three-dimensional volume. If we call Q the instanton density in a three-volume $dx_1 dx_2 dx_3$, we have the relation

$$Q = \int dx_4 \frac{1}{32\pi^2} F^a_{\mu\nu} \tilde{F}^{\mu\nu a} = \frac{B}{8\pi^2 R_3}. \tag{2.10}$$

We count the number of parameters of the solution. In total there are four parameters, l, B, R_3, d, and two relations between them, (2.3), (2.9). Moreover, we want the instanton charge (2.10) to be fixed. We thus remain with a one-parameter family of solutions, which we can take to be the separation d. Rewriting everything as a function of the distance d, the coupling g, and the instanton charge density Q, we have the following set of relations:

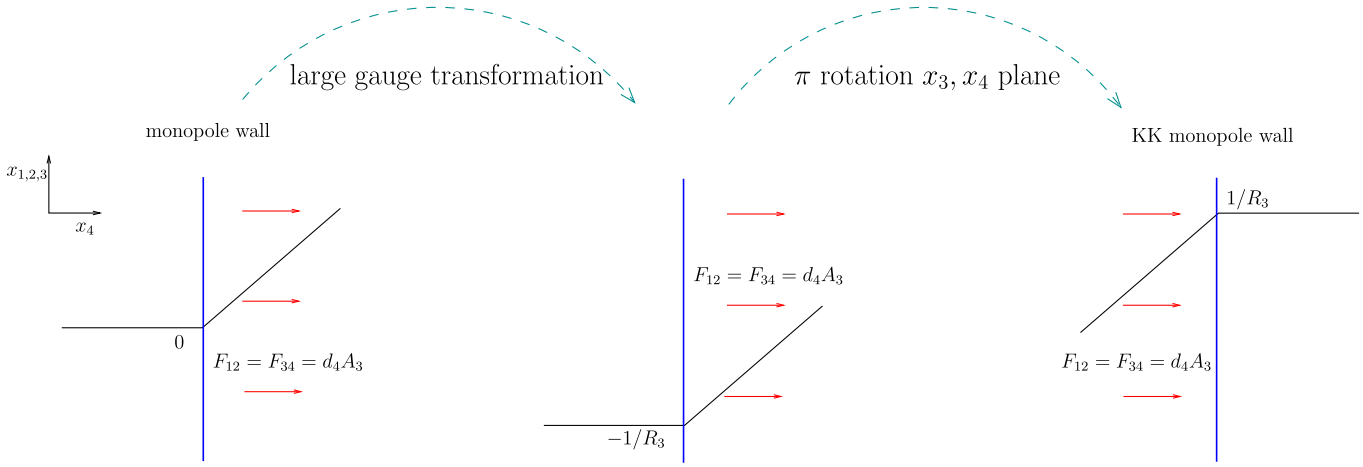

FIG. 2 (color online). Sequence of transformations from monopole wall to KK monopole wall, first the large-gauge transformation and then the π rotation in the x_3, x_4 plane.

$$\delta \simeq l = \frac{2\sqrt{\pi}}{\sqrt{B}} \qquad R_3 = \frac{1}{2\pi\sqrt{2Qd}} \qquad B = 2\pi\sqrt{\frac{2Q}{d}}. \tag{2.11}$$

The instanton bag we just discussed is very similar to the composite monopole walls studied in [18–21]. These solutions have a hyper-Kahler moduli space which, for two walls only, is $4+4$ dimensional. The relative 4 moduli are distance d. a $U(1)$ relative phase, and a shift in the lattice positions of the two walls. The distance d is, for the present paper, the only modulus of these four that we will consider because the others affect only the microscopic structure.

For the bag approximation to be valid, we want to be in a regime in which we can neglect the microscopic structure of the wall, and thus we want the distance d to be much greater than l and δ. The most stringent condition of the two's is

$$d \gg l \Rightarrow \sqrt[4]{d^3 Q} \gg 1. \tag{2.12}$$

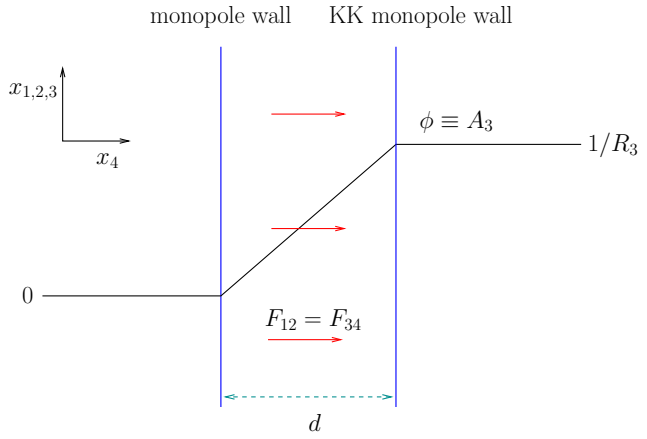

FIG. 3 (color online). Monopole wall and KK monopole wall with instanton charge inside the two plates.

Note that, even by keeping fixed Q and g, we can always reach a point in the moduli space where d is large enough to make the approximation valid. Yet another way to satisfy the condition is to increase Q while keeping d and g fixed.

It may be instructive to avoid the direct use of the Bogomol'nyi equation (2.9) and use instead the minimization of the energy. The energy density per unit of volume $dx_1 dx_2 dx_3$ is

$$E = \frac{1}{2g^2}\int_{-d/2}^{d/2} dx_4 ({F^a_{12}}^2 + {F^a_{34}}^2), \tag{2.13}$$

which then becomes

$$E = \frac{1}{2g^2}\left(dB^2 + \frac{64\pi^4 Q^2}{dB^2}\right). \tag{2.14}$$

Minimizing by keeping Q fixed, we determine the value of dB^2 and the corresponding energy density

$$dB^2 = 8\pi^2 Q \qquad E = \frac{8\pi^2 Q}{g^2}, \tag{2.15}$$

where (2.9) is recovered, and one parameter between d and B disappears from E and remains thus a free modulus. This minimization strategy is the same that we will use in Sec. IV in the HQCD context, where the BPS equation is no longer valid.

A brane construction in string theory provides a very intuitive realization of the monopole wall [4,26]. Monopoles are realized as D1-strings stretched between two D3-branes in type IIB string theory. We may take the D3 world volume to be stretched along the directions $x_{0,1,2,4}$ and the D1-string along $x_{0,3}$ with the two D3-branes separated in the x_3 direction. A monopole wall, in its simplest lattice realization, is an $\mathbb{R}^2$ periodic configuration, which we take along $x_{1,2}$. A series of transformations brings

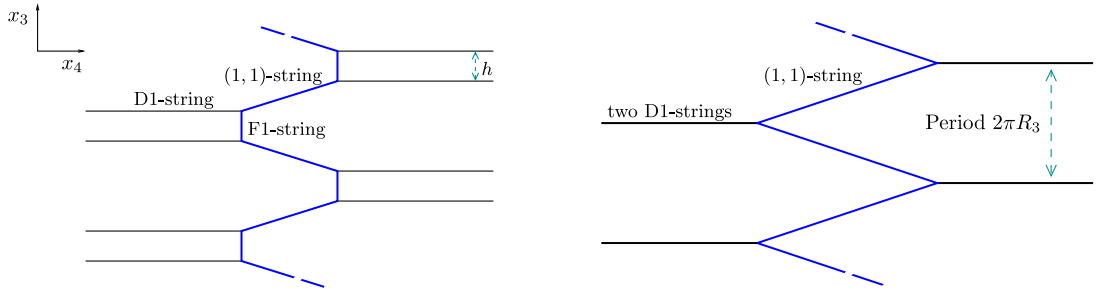

FIG. 4 (color online). Web of string junctions in the $x_{3,4}$ plane. The basic constituent is the three string junction D1-F1-(1,1). The structure is periodic in the x_3 direction. The second is the web for the limit of coincident D1-strings. This configuration corresponds to the instanton bag of Fig. 3.

this configuration to a simpler system. First it can be turned into a D3-F1 system by an S-duality. Then, because we take a periodic configuration along x_{12}, we can compactify on a torus and perform T-duality on both directions. After these transformations, the D3-brane becomes a D1-string along the directions $x_{0,4}$, and the D1-string becomes a fundamental F1-string along $x_{0,3}$. The monopole wall is thus transformed into a web of connected D1 and F1 strings periodic in x_3. The basic building block of this web is a string junction among a D1, an F1, and a third dyonic (1,1)-string with a certain angle in the $x_{3,4}$ plane dictated by the balance of the tensions. The instanton bag configuration is then described by the web in Fig. 4. The junctions have to be placed in a periodic configuration in x_3 with the chain resulting from the KK monopole wall shifted of a half-period amount with respect to the chain coming from the monopole wall. To obtain the instanton bag we take this periodic web of string junctions, and perform all the previous dualities in reverse order. When we arrive at the original D3-D1 configuration, we perform another T-duality in the direction x_3 and we get the D4-D0 system.

As it is clear from the string web illustration in Fig. 4, the monopole wall does not necessarily have to have a zero Higgs field on its empty side. The value of the Higgs field is in fact another parameter, which we call h (the existence of this extra freedom was observed in [18]). For $h \neq 0$, the monopole wall has an intrinsic tension given by

$$T = \frac{Bh}{g^2} = \frac{M_{\rm mon}}{l^2}, \tag{2.16}$$

which is consistent with the mass of a single BPS monopole with an asymptotic Higgs field equal to h

$$M_{\rm mon} = \frac{4\pi h}{g^2}. \tag{2.17}$$

The two configurations in Fig. 4 have exactly the same energy. What is gained from the monopoles' mass is lost from the fact that the two walls are closer. In HQCD, this is no longer a free modulus, but must enter the minimization procedure like d and B. We will see that the $h = 0$ is, in general, the energetically favorite state.

We conclude this section with a discussion of the gauge in which we want to prepare our system. When we embed the monopole wall and KK monopole wall pair in holography, we want to choose a gauge that is the most convenient for the AdS/CFT dictionary. Usually, this is the gauge in which the gauge field is zero at the UV boundary, which is the two asymptotic limits $x_4 \to \pm\infty$.[1] The gauge we used for the previous discussion is not of this kind because there are Dirac string singularities, one for every period of the monopole wall and KK monopole wall. To eliminate the Dirac strings we can go to the analogue of the hedgehog gauge for the 't Hooft–Polyakov monopole. In the middle of the two walls, the gauge transformation is a function $U(x_1, x_2)$ so that the adjoint field $U(x_1, x_2)t_{\rm su(2)}U(x_1, x_2)^{-1}$ winds around $SU(2)/U(1)$ once for every period of the wall lattice. This is particularly relevant for later application in HQCD. The magnetic fields F_{12} and F_{34} fluctuate around the su(2) algebra so that every wave coming from the empty side of the wall in a fixed su(2) generator (which in HQCD are dual to the vector meson states in a given isospin state) interacts with some magnetic field. This gauge is convenient for checking that the instanton charge is equal to the flux of the Chern-Simons current

$$K^\mu = \frac{1}{16\pi^2}\epsilon^{\mu\nu\rho\sigma}\left(A^a_\nu F^a_{\rho,\sigma} + \frac{2}{3}\epsilon_{abc}A^a_\nu A^b_\rho A^c_\sigma\right). \tag{2.18}$$

We take a 4D volume as in Fig. 5 that encloses part of the instanton bag. The gauge field vanishes at the left side of the monopole wall and at the right side of the KK monopole wall. So the Chern-Simons flux can escape only through the volumes 1-3-4, 2-3-4, and 1-2-4 inside the two walls. No term from ϵ_{abc} in the Chern-Simons current gives any contribution. Moreover, there is no contribution from the

[1]If the gauge field is not zero at the boundary but the gauge is equivalent to zero, and if we do not want to interpret it as a source, the AdS/CFT dictionary also must be modified accordingly.

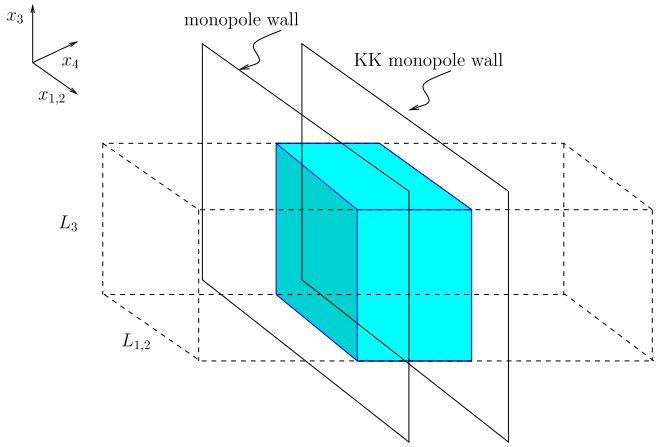

FIG. 5 (color online). Check of the Chern-Simons flux.

1-2-4 volume. We just have to compute the flux from 1-3-4 and 2-3-4. The total instanton charge I is then

$$I = \int dx_i dx_3 dx_4 \frac{1}{8\pi^2} A_i^a F_{34}^a = \frac{B}{8\pi^2 R_3} L_1 L_2 L_3, \quad (2.19)$$

where $i = 1, 2$. This is consistent with the instanton density (2.10).

III. HQCD AND FINITE BARYON DENSITY

The Sakai-Sugimoto model, at low energy, consists of a $U(2)$ gauge theory in the following 5D warped metric background:

$$ds^2 = H(z) dx_\mu dx^\mu + H(z)^{-1} dz^2$$
$$H(z) = \left(1 + \frac{z^2}{z_0^2}\right)^{2/3}. \quad (3.1)$$

The length scale z_0 is related to the inverse of the dynamical scale in the dual QCD-like theory. From now on we set $z_0 = 1$. The action is a sum of the Yang-Mills term plus a $U(2)$ Chern-Simons term:

$$S = -\frac{N_c \lambda}{216\pi^3} \int d^4x dz \sqrt{-g} \frac{1}{2} \mathrm{tr}(\mathcal{F}_{\Gamma\Delta} \mathcal{F}^{\Gamma\Delta}) + \frac{N_c}{24\pi^2} \int d^4x dz \omega_5(\mathcal{A}). \quad (3.2)$$

We use the index conventions as follows: $\Gamma, \Delta, \ldots = 0, 1, 2, 3, z$; $\mu, \nu, \ldots = 0, 1, 2, 3$; $I, J = 1, 2, 3, 4$ and $i, j, \ldots = 1, 2, 3$. The factors N_c and λ are, respectively, the number of colors and the 't Hooft coupling of the dual theory. We can decompose the gauge field into non-Abelian and Abelian components $U(2) = SU(2) \times U(1)$:

$$\mathcal{A}_\Gamma = A_\Gamma + \frac{1}{2}\hat{A}_\Gamma \qquad \mathcal{F}_{\Gamma\Delta} = F_{\Gamma\Delta} + \frac{1}{2}\hat{F}_{\Gamma\Delta}. \quad (3.3)$$

In the following, we are only interested in static configurations, so we restrict to the following ansatz:

$$A_I, \hat{A}_0 = A_I(x_I), \hat{A}_0(x_I) \qquad A_0, \hat{A}_I = 0, 0. \quad (3.4)$$

The action is then reduced to

$$\mathcal{S} = \int d^4x dz \left\{ \frac{1}{2H^{1/2}} (\partial_i \hat{A}_0)^2 + \frac{H^{3/2}}{2} (\partial_z \hat{A}_0)^2 - \frac{1}{2H^{1/2}} \mathrm{tr}(F_{ij}^2) - H^{3/2} \mathrm{tr}(F_{iz}^2) \right\} + \frac{1}{\Lambda} \int d^4x dz \hat{A}_0 \mathrm{tr}(F_{IJ} F_{KS}) \epsilon^{IJKS}, \quad (3.5)$$

where we have rescaled for convenience the action and the 't Hooft coupling as

$$\mathcal{S} = \frac{64\pi^2}{\Lambda N_c} S \quad \text{and} \quad \Lambda = \frac{8\lambda}{27\pi}. \quad (3.6)$$

For large 't Hooft coupling, the Chern-Simons term is parametrically suppressed with respect to the Yang-Mills term. The instanton in the large Λ limit can thus be approximated by a BPS ansatz [27,28]

$$A_I = -\sigma_{IJ} x_J \frac{1}{\rho^2 + l^2}, \quad (3.7)$$

with $\sigma_{ij} = \epsilon_{ijk}\sigma_k$ and $\sigma_{iz} = -\sigma_{zi} = \sigma_i$. The size of the instanton l is then obtained by minimizing the energy restricted to the BPS moduli space. This gives

$$l = \frac{3^{1/4} 2^{7/4}}{5^{1/4} \Lambda^{1/2}} \quad \text{and} \quad \mathcal{E} = 8\pi^2 \left(1 + \frac{2^{7/2}}{15^{1/2}\Lambda} + \cdots\right). \quad (3.8)$$

At large Λ, the size of the instanton is much smaller that the curvature scale of the metric,[2] which is why the BPS profile function provides a good approximation of the true solution, at least in the almost-flat region of the metric. Moreover, the correction to the BPS mass is a subleading term of order $\mathcal{O}(1/\Lambda)$. The solution flows exactly to the BPS for $\Lambda \to \infty$ but only in rescaled coordinates [29], so the long-distance properties are not captured by the BPS ansatz. Long-distance properties are not relevant for high-density QCD due to the small distance between baryons, so we will not discuss them in this paper.

At finite densities, the instantons are distributed on a lattice configuration, and they begin to populate the 3D space by all sitting at the bottom of the gravitational potential at $z = 0$. Their average distance is thus $d = Q^{-1/3}$, where Q is the 3D instanton density. This

[2]Upon substitution, $l = 3^{7/4}\pi^{1/2}2^{1/4}/5^{1/4}\lambda^{1/2}$, which is consistent with the results in the literature [27–30].

configuration remains valid as long as the typical distance d is longer than the size of the single instantons, and thus for densities $Q \ll \Lambda^{3/2}$. In this regime, the energy density is dominated by the BPS term and is thus linear in Q. In the ensemble in which we keep the chemical potential fixed, a phase transition to hadronic matter is expected to take place when the average distance is of order of the curvature scale; thus, $Q \simeq 1$. This is when the attractive force due to the pion-pion tail is comparable with the Coulomb repulsive force [31]. Above this scale $Q \gg 1$, the attractive force becomes irrelevant with respect to the Coulomb repulsive force. The Coulomb interaction, for any couple of instantons at distance $\tilde{d}$, is order $E_{\text{Coulomb}} \propto 1/\Lambda^2\tilde{d}^2$ and this is valid for $l \ll \tilde{d} \ll 1$. The $1/\tilde{d}^2$ dependence is because we are in $4+1$ dimensions and the $1/\Lambda^2$ dependence is because $1/\Lambda$ is the analogue of the electric charge. We can compute the energy density of the 3D lattice as a sum of the mass of the single constituents plus the correction due to the Coulomb interaction:

$$\mathcal{E} = 8\pi^2 Q\left(1 + \mathcal{O}\left(\frac{Q}{\Lambda^2}\right)\right). \tag{3.9}$$

Note that, for the Coulomb term, we summed the $1/\Lambda^2\tilde{d}^2$ term for every pair of constituents, taking as cutoff $\tilde{d} \simeq 1$, where the Coulomb law is certainly modified by the metric curvature. The Coulomb correction becomes comparable with the BPS energy at densities of order $Q \simeq \Lambda^2$, which are much bigger than $\Lambda^{3/2}$.

When the instanton density becomes of order $Q \simeq \Lambda^{3/2}$, two interesting things happen almost simultaneously. First, the instanton lattice is no longer diluted because the typical inner distance becomes comparable with the instanton size $d \simeq l$. Second, the instantons begin to climb the holographic direction as we are going to see with the following simple estimate. We can estimate the force acting on each single instanton. The first force is the gravitational one, $F_{\text{Grav}} \propto -\Lambda z$, where z is the linear displacement around the bottom of the gravitational potential. Then there is a Coulomb force due to the surrounding instantons in the 3D lattice. This force, projected in the z component, is proportional to $z/\tilde{d}^4$ for any pair of instantons. The total force is thus $F_{\text{Coulomb}} \propto +Q^{4/3}z$. This force is pulling the instantons away from the bottom of the gravitational potential because it is repulsive. The instantons begin to move away from the bottom of the gravitational potential when the two forces are comparable $F_{\text{Grav}} \simeq F_{\text{Coulomb}}$. This condition is the same as the breaking of the diluted approximation. The fact that these two changes both happen at the densities $Q \simeq \Lambda^{3/2}$ is not a coincidence; it has also been discussed in [32] and observed in the toy model [1]. The agents that stabilize the instanton radius are, in fact, the same that decide when the instanton lattice prefers to move the holographic direction.

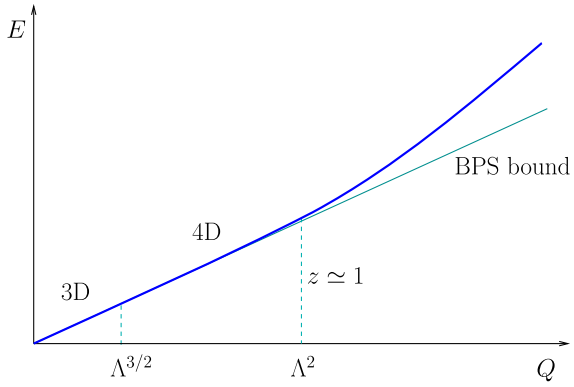

FIG. 6 (color online). Generic expectation for the energy density of the HQCD phases as function of instanton density Q.

At densities $Q \simeq \Lambda^{3/2}$, the instantons start to fill the holographic direction as well. After that, another transition happens at higher densities $Q \simeq \Lambda^2$. Assuming the average distance remains of the order of the instanton scale $d \simeq l$, the instanton 4D lattice boundary reaches the curvature scale $z \simeq 1$, which is when Q is of order Λ^2. This is also the density when the Coulomb energy becomes comparable with the BPS energy (3.9), and thus the energy density strongly deviates from the BPS bound. These phases are summarized in Fig. 6.

The information we extracted so far is based on qualitative estimates. To find the actual instanton solution for the high-density phase is a much harder task. A 4D instanton lattice is specified by many parameters: the 3D lattice strata, the relative orientation of the instantons in the internal space, the sizes of the instantons, and the depth of the various layers in the holographic direction z. For densities $Q \ll \Lambda^2$, the problem simplifies since we can use a BPS ansatz and minimize the energy restricted to the BPS moduli space. But even in this simplified case, the problem remains difficult to solve in full generality. Some results of the self-dual configurations periodic on $\mathbb{T}^3$ and $\mathbb{T}^4$ have been obtained using a version of the ADHM transform [33]. But the energy minimization would require knowledge of the actual gauge fields and not just the ADHM data.

Our strategy in the rest of the paper is to use the instanton bag discussed in Sec. II as an ansatz for the high-density phase. For the instanton bag approximation, we can compute the fields and thus perform the energy minimization. At the moment, we do not have sufficient control over other possible instanton configurations to compute their energy and thus decide which is the actual minimum for the high-density phase.

IV. INSTANTON BAG EMBEDDED IN THE SAKAI-SUGIMOTO MODEL

We now embed the instanton bag studied in Sec. II into the Sakai-Sugimoto model.

We first use the BPS ansatz and find the best values of the moduli that minimize the energy density at a fixed instanton density. The BPS solution in flat space has two free moduli, the wall separation d and Higgs field h. We now parametrize them with $\pm z_W$, which are the positions of the monopole wall and KK-monopole wall in the z direction, and Δ, which is the amount of instanton charge carried by the walls as a delta function. The relation

$$Q = \frac{B^2 z_w}{4\pi^2} + \Delta \tag{4.1}$$

is valid for a self-dual solution and gives the instanton charge Q as function of z_w, B, and Δ. We use it later to express B as function of the other parameters.

The action (3.5) inside the two walls is reduced to

$$\frac{\mathcal{S}}{V_3} = \int dt \int_{-z_w}^{z_w} dz \left\{ \frac{H^{3/2}}{2} (\partial_z \hat{A}_0)^2 - \frac{B^2(1+H^2)}{2H^{1/2}} + \frac{4}{\Lambda} \hat{A}_0 B^2 \right\}. \tag{4.2}$$

From this, we find the equation for the Abelian electric potential $\hat{A}_0$:

$$\partial_z (H^{3/2} \partial_z \hat{A}_0) - \frac{4}{\Lambda} B^2 = 0. \tag{4.3}$$

The solution for the electric field inside the walls is thus

$$\partial_z \hat{A}_0 = \frac{4B^2 z}{\Lambda(1+z^2)} \quad \text{for } |z| \le z_w. \tag{4.4}$$

The solution outside the walls is given by the solution of the equation without sources, matched with (4.4) at $z = z_w$:

$$\partial_z \hat{A}_0 = \frac{16\pi^2 Q}{\Lambda(1+z^2)} \quad \text{for } |z| > z_w. \tag{4.5}$$

The energy density is given by the sum of three contributions:

$$\mathcal{E} = \int_0^{z_w} \left(H^{3/2} (\partial_z \hat{A}_0)^2 + \frac{B^2(1+H^2)}{H^{1/2}} \right) + 8\pi^2 \Delta (1 + z_w^2) + \int_{z_w}^{\infty} H^{3/2} (\partial_z \hat{A}_0)^2, \tag{4.6}$$

with $A_0(z)$ given by (4.4) and (4.5). We evaluate the integrals, and then expand in series of z_w, since the self-dual approximation is supposed to be valid only for $z_w \ll 1$. The result is

$$\mathcal{E}(Q; z_w, \Delta) = 8\pi^2 Q + \frac{128\pi^5 Q^2}{\Lambda^2} - \frac{256(2\pi^4 Q^2 + 2\pi^4 Q\Delta - \pi^4 \Delta^2)}{3\Lambda^2} z_w + \frac{8\pi^2 (Q + 8\Delta)}{9} z_w^2 + \cdots \tag{4.7}$$

This energy density has to be minimized with respect to z_w and Δ by keeping the instanton charge Q fixed. The solution is given by

$$z_w = \frac{96\pi^2 Q}{\Lambda^2} \quad \Delta = 0. \tag{4.8}$$

The energy density evaluated at the minimum is then

$$\mathcal{E}(Q) = 8\pi^2 Q \left(1 + \frac{16\pi^3 Q}{\Lambda^2} - \frac{1024\pi^4 Q^2}{\Lambda^4} + \cdots \right). \tag{4.9}$$

Note that the dominant term is the BPS bound, and the corrections are small if $Q \ll \Lambda^2$. This is also the regime in which $z_w \ll 1$. Moreover, the bag approximation is valid when the wall microscopic structure is much smaller than z_w [see (2.12)] and thus, using (4.8), becomes equivalent to $Q \gg \Lambda^{3/2}$. Therefore, the BPS and bag approximations are both valid in the region of instanton densities $\Lambda^{3/2} \ll Q \ll \Lambda^2$.

In the previous analysis we used the canonical ensemble: we kept fixed the charge density Q and minimized the energy density. We can also pass from the canonical to the grand-canonical ensemble. The first way is to recover the chemical potential with the usual thermodynamic relation

$$\mu_Q = \frac{\partial \mathcal{E}(Q)}{\partial Q} = 8\pi^2 + \frac{256\pi^3 Q}{\Lambda^2} - 24 * 1024 \frac{\pi^6 Q^2}{\Lambda^4} + \cdots \tag{4.10}$$

The second way, by using the AdS/CFT prescription, is to compute the asymptotic value of $\hat{A}_0$. This can be done by integrating the electric field in the two regions (4.4) and (4.5). The result is

$$\hat{A}_0(\infty) = \hat{A}_0(0) + \frac{8\pi^3 Q}{\Lambda} - \frac{768\pi^4 Q^2}{\Lambda^3} + \cdots, \tag{4.11}$$

where we have kept the first two orders on Q/Λ^2. To compare it with the chemical potential, we first have to find the proper normalization. The electromagnetic coupling comes from the Chern-Simons term of the action (3.5)

$$\mathcal{S}_{\rm CS} = \frac{1}{\Lambda} \int d^4x dz \hat{A}_0 \mathrm{tr}(F_{IJ} F_{KS}) \epsilon^{IJKS} = \int dt \frac{32\pi^2}{\Lambda} \hat{A}_0 Q, \tag{4.12}$$

so the AdS/CFT prescription predicts the following relation between chemical potential μ_Q and the asymptotic value of $\hat{A}_0$:

$$\mu_Q = \frac{32\pi^2}{\Lambda}\hat{A}_0(\infty). \tag{4.13}$$

We can then see that the two ways to compute μ_Q, (4.10) and (4.13), agree to every order if we choose $\hat{A}_0(0) = \frac{\Lambda}{4}$.

When z_w becomes of order 1, we can no longer use the self-dual approximation, although we can still use the instanton bag approximation. For this, we have to solve the profile function for $A_3(z)$ as it is generally modified by the metric curvature and is no longer linear in z. The relation (4.1) is now given in more generality by the following:

$$Q = \frac{B}{8\pi^2}\int_{-z_w}^{z_w}\partial_z A_3 + \Delta. \tag{4.14}$$

The action density between the two walls is

$$\frac{\mathcal{S}}{V_3} = \int dt \int_{-z_w}^{z_w} dz \left\{ \frac{H^{3/2}}{2}(\partial_z \hat{A}_0)^2 - \frac{B^2}{2H^{1/2}} - \frac{H^{3/2}}{2}(\partial_z A_3)^2 + \frac{4}{\Lambda}\hat{A}_0 B \partial_z A_3 \right\}, \tag{4.15}$$

from which we derive the equations for $\hat{A}_0$ and A_3:

$$\partial_z(H^{3/2}\partial_z\hat{A}_0) - \frac{4}{\Lambda}B\partial_z A_3 = 0 \tag{4.16}$$

$$\partial_z\left(H^{3/2}\partial_z A_3 - \frac{4}{\Lambda}\hat{A}_0 B\right) = 0. \tag{4.17}$$

The second one can be integrated

$$\partial_z A_3 = \frac{4\hat{A}_0 B - C\Lambda}{\Lambda H^{3/2}}, \tag{4.18}$$

where C is an arbitrary integration constant. Equation (4.16), together with the boundary condition $\partial_z\hat{A}_0(0) = 0$, gives the solutions for $\hat{A}_0$:

$$\hat{A}_0 = \hat{A}_0(0) + \frac{C\Lambda}{4B}\left(1 - \cosh\left(\frac{4B\tan^{-1}(z)}{\Lambda}\right)\right). \tag{4.19}$$

The solution for $\partial_z A_3$ is

$$\partial_z A_3 = -\frac{C}{H^{3/2}}\cosh\left(\frac{4B\tan^{-1}(z)}{\Lambda}\right). \tag{4.20}$$

The relation (4.14) can now be written as

$$Q = \frac{C\Lambda}{16\pi^2}\sinh\left(\frac{4B\tan^{-1}(z_w)}{\Lambda}\right) + \Delta. \tag{4.21}$$

Outside the walls, A_3 is constant, while $\hat{A}_0$ is given by

$$\hat{A}_0 = c_1 - C\sinh\left(\frac{4B\tan^{-1}(z_w)}{\Lambda}\right)\tan^{-1}(z), \tag{4.22}$$

where c_1 is a constant that we do not need for the moment.

The energy density is then given by

$$\mathcal{E} = \int_0^{z_w}\left(H^{3/2}(\partial_z\hat{A}_0)^2 + \frac{B^2}{H^{1/2}} + H^{3/2}(\partial_z A_3)^2\right) + \frac{\Delta(1+z_w^2)}{\pi^2} + \int_{z_w}^{\infty} H^{3/2}(\partial_z\hat{A}_0)^2. \tag{4.23}$$

We can use the relation (4.21) to write the integration constant C as function of the other parameters, and then the energy density becomes

$$\mathcal{E}(Q;B,z_w,\Delta) = \frac{32\pi^4(Q-\Delta)^2\sinh\left(\frac{8B\tan^{-1}(z_w)}{\Lambda}\right)}{B\Lambda\left(\sinh\left(\frac{4B\tan^{-1}(z_w)}{\Lambda}\right)\right)^2} + B^2\int_0^{z_w}\frac{1}{(1+z^2)^{1/3}} + \frac{\Delta(1+z_w^2)}{\pi^2} + \frac{256\pi^4(Q-\Delta)^2}{\Lambda^2} \times\left(\frac{\pi}{2} - \tan^{-1}(z_w)\right). \tag{4.24}$$

This is the function that has to be minimized with respect to the three parameters B, z_w, Δ, while keeping Q fixed. With the following convenient rescaling

$$B = b\Lambda \qquad Q = q\Lambda^2, \tag{4.25}$$

we can write the functional (4.24) as

$$\frac{1}{\Lambda^2}\mathcal{E}(q;b,z_w) = \frac{32\pi^4 q^2\sinh\left(8b\tan^{-1}(z_w)\right)}{b\left(\sinh\left(4b\tan^{-1}(z_w)\right)\right)^2} + b^2\int_0^{z_w}\frac{1}{(1+z^2)^{1/3}} + 256\pi^4 q^2\left(\frac{\pi}{2} - \tan^{-1}(z_w)\right). \tag{4.26}$$

Numerical examples, for a given value of q, show that the minimum always exists and is at $\Delta = 0$ for some finite value of B, z_w.

An analytic solution to the minimization of (4.26) can be obtained in the limit $z_w \gg 1$. For this, we can first minimize (4.26) with respect to z_w by keeping only the dominant terms in a large z_w expansion,

$$z_w = 64\pi^3\left(\frac{q\coth(2b\pi)}{b}\right)^{3/2} \quad \text{for } z_w \gg 1. \tag{4.27}$$

We then have to minimize

$$\frac{1}{\Lambda^2}\mathcal{E}(q;b) = \frac{64\pi^4 q^2 \coth(2b\pi)}{b} + 16b^{3/2}\pi(q^2(\coth(2b\pi))^2)^{1/4} \quad (4.28)$$

with respect to b. By considering only the dominant terms in the large q limit, we obtain the result

$$b = \frac{22^{1/5}\pi^{6/5}q^{3/5}}{3^{2/5}} \quad \text{and} \quad z_w = 162^{1/5}3^{3/5}\pi^{6/5}q^{3/5} \quad \text{for } q \gg 1, \quad (4.29)$$

and the energy density is

$$\mathcal{E}(Q) = 80\left(\frac{2^4\pi^{14}Q^7}{3^3\Lambda^4}\right)^{1/5} \quad \text{for } Q \gg \Lambda^2. \quad (4.30)$$

Note that the derivative with respect to Δ is positive:

$$\left.\frac{\partial\mathcal{E}}{\partial\Delta}\right|_{\Delta=0} \simeq +\frac{z_w^2}{\pi^2} - \frac{256\pi^5 Q}{\Lambda^2} > 0 \quad \text{for } Q \gg \Lambda^2. \quad (4.31)$$

This limit $Q \gg \Lambda^2$ is exactly the opposite of the BPS limit previously considered. We can compute the chemical potential in this limit with the thermodynamic relation

$$\mu_Q = \frac{\partial\mathcal{E}(Q)}{\partial Q} = \frac{1122^{4/5}\pi^{14/5}Q^{2/5}}{3^{3/5}\Lambda^{4/5}}. \quad (4.32)$$

The asymptotic value $\hat{A}_0$ is obtained by integrating (4.19) and (4.22):

$$\hat{A}_0(\infty) = 16\pi^2 Q\left(\frac{1}{4B} + \frac{1}{z_w}\right) = \frac{7\pi^{4/5}\Lambda^{1/5}Q^{2/5}}{2^{1/5}3^{3/5}}, \quad (4.33)$$

and this agrees with (4.32) by using (4.13).

The minimization can be performed numerically for any value of Q. The results are shown in Figs. 7 and 8 and are confronted both with the small Q and large Q approximations.

We can consider a local inertial frame by zooming in closer to the monopole wall. In the new coordinates,

$$\tilde{x}_\mu = H(z_w)^{1/2}x_\mu \qquad \tilde{z} = \frac{z - z_w}{H(z_w)^{1/2}}, \quad (4.34)$$

the metric is locally Minkowski,

$$ds^2 \simeq d\tilde{x}_\mu d\tilde{x}^\mu + d\tilde{z}^2, \quad (4.35)$$

and this is valid as long as $|\tilde{z}|$ is much smaller than the metric curvature radius, which, for $z_w \gg 1$, is the condition

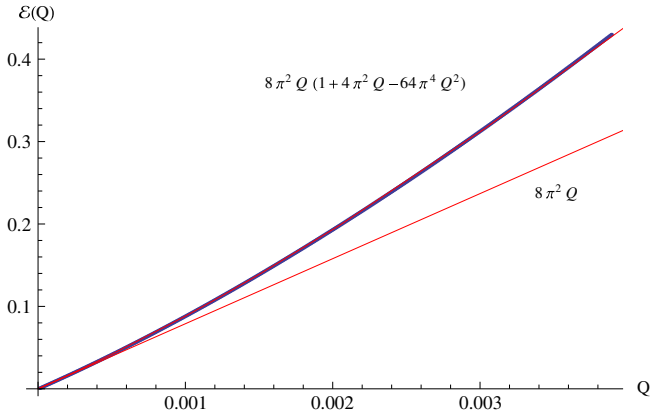

FIG. 7 (color online). Numerical plot of $\mathcal{E}(Q)$ for small values of Q obtained from the minimization of (4.26) for $\Lambda = 2$. This confirms the expectation from the BPS approximation (4.9).

$$|\tilde{z}| \ll \frac{1}{|R|^{1/2}} \simeq \frac{3z_w^{1/3}}{2\sqrt{13}}. \quad (4.36)$$

In this frame, the fields close to the wall are

$$F_{\tilde{z}\tilde{3}} = F_{z3} = \frac{8\pi^2 Q}{\Lambda z_w^2} = \frac{\pi^{28/5}\Lambda^{7/5}}{3^{6/5}8Q^{1/5}}$$
$$F_{\tilde{1}\tilde{2}} = \frac{B}{H(z_w)} = \frac{\pi^{18/5}\Lambda^{7/5}}{3^{6/5}8Q^{1/5}}. \quad (4.37)$$

The monopole wall lattice period $\tilde{l}$ and the transverse thickness $\tilde{\delta}$ are given by

$$\tilde{l} = \frac{1}{\sqrt{F_{\tilde{1}\tilde{2}}}} \qquad \tilde{\delta} = \frac{1}{\sqrt{F_{\tilde{z}\tilde{3}}}} \quad (4.38)$$

and are always smaller than the curvature radius. This justifies the approximation made before of neglecting the microscopic structure of the walls.

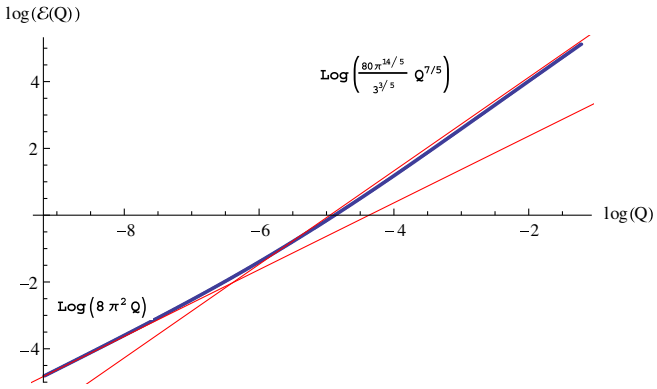

FIG. 8 (color online). Numerical solution of $\mathcal{E}(Q)$ in a log-log plot for $\Lambda = 2$. This shows the interpolation between the almost-BPS limit for small Q and the asymptotic solution (4.30) for large Q.

V. EMBEDDING IN STRING THEORY

Now we move to the full string version of Sakai-Sugimoto (SS) [34]. First we briefly review the brane construction and the near-horizon geometry. The SS model starts with the intersection of D4, D8, and anti-D8 branes in type IIA string theory. The gauge theory with group $SU(N_c)$ is defined on the D4-branes, which are extended along the directions $x_{0,1,2,3,5}$, and the N_f flavors are provided by the D8-branes and anti-D8-branes extended along the directions $x_{0,1,2,3,5,6,7,8,9}$. This brane intersection leaves only massless chiral fermions with one gauge and one flavor index in the low-energy theory. Moreover, the direction x_5 is compactified with antiperiodic boundary conditions for fermions on a circle with radius R_5 [35]. With this compactification, the low-energy of the D4 is exactly that of QCD in $3+1$ dimensions with N_f massless fermions.

The next step is to take large N_c and large λ limits and go to near-horizon geometry of the D4-branes. The D4-branes disappear and leave a curved AdS_5 geometry compactified on x_5, plus an S^4 sphere with N_c units of Ramond-Ramond flux. The D8-branes remain as physical branes in this background. The geometry, the field strength, and the dilaton are given by

$$\begin{aligned} ds^2 &= \left(\frac{u}{L}\right)^{3/2}(dx_\mu dx^\mu + h(u)dx_5^2) \\ &\quad + \left(\frac{L}{u}\right)^{3/2}\left(\frac{du^2}{h(u)} + u^2 d\Omega_4^2\right) \\ F_4 &= \frac{(2\pi)^3\alpha'^{3/2}N_c}{V_4}\,\mathrm{vol}(S^4) \\ e^{\phi} &= g_s\left(\frac{u}{L}\right)^{3/4}, \end{aligned} \tag{5.1}$$

with

$$h(u) = 1 - \left(\frac{u_0}{u}\right)^3. \tag{5.2}$$

This is a cigarlike topology in the two-dimensional subspace x_5, u (see Fig. 9). It is like a Euclidean Schwarzschild black hole, with x_5 playing the role of the Euclidean time. The holographic direction is u, and both limits $u \to \pm\infty$ correspond to the UV limit of the boundary theory. The cigar topology implies that the two stacks of D8 and anti-D8 branes are continuously joined together at the tip of the cigar; this is the geometric realization of chiral symmetry breaking.

We now recall the relation between bulk and boundary theories. The dual gauge theory is defined by the gauge couplings g_{YM4} and g_{YM4}, the number of colors N_c, the compactification radius R_5, and the 't Hooft coupling λ related by the following:

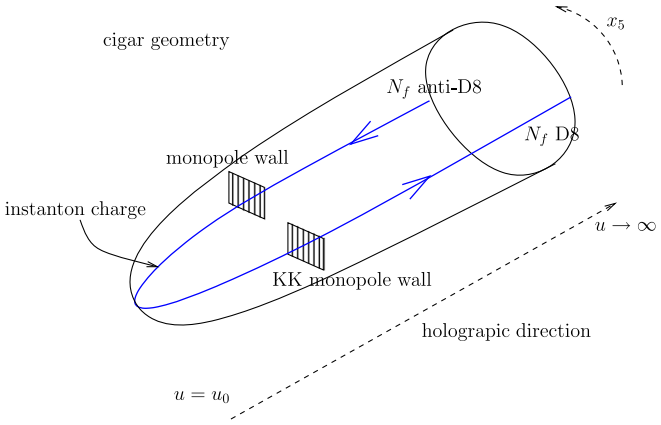

FIG. 9 (color online). Geometric realization of confinement and chiral symmetry breaking in the Sakai-Sugimoto model and the embedded instanton bag on the $D8$'s worldvolume.

$$g_{YM4}^2 = \frac{g_{YM5}^2}{2\pi R_5} \qquad \lambda = g_{YM4}^2 N_c. \tag{5.3}$$

The dynamical scale is given by

$$\Lambda_{\mathrm{QCD}} = \frac{1}{R_5}e^{-\mathrm{cost}/\lambda} \tag{5.4}$$

which means that the low-energy QCD is hierarchically separated from the Kaluza-Klein modes only for $\lambda \ll 1$. This is one limitation of the $\lambda \to \infty$ limit in the SS model. Thus, the bulk string theory has parameters g_s, α', L, u_0, and R_5. The absence of any conical singularity at the cigar tip gives the relation

$$\frac{1}{R_5^2} = \frac{9u_0}{4L^3}. \tag{5.5}$$

We then have three parameters to be matched between bulk and boundary. The dictionary is given by the following three relations:

$$\frac{L^3}{\alpha'} = \frac{\lambda R_5}{2} \qquad \frac{u_0}{\alpha'} = \frac{2\lambda}{9R_5} \qquad g_s\sqrt{\alpha'} = \frac{\lambda R_5}{2\pi N_c}. \tag{5.6}$$

Note that only three out of the four parameters, L, u_0, g_s, α', are needed to define the boundary parameters N_c, λ, R_5.

To maintain string theory at weak coupling, we need the curvature of the bulk to be small with respect to the string scale and thus the 't Hooft coupling to be large:

$$\frac{\sqrt[4]{L^3 u_0}}{\sqrt{\alpha'}} \gg 1 \Rightarrow \sqrt{\lambda} \gg 1. \tag{5.7}$$

Moreover, the string coupling has to be small:

$$g_s\left(\frac{u_0}{L}\right)^{3/4} \gg 1 \Rightarrow \sqrt{\lambda^{3/2}/N_c} \ll 1. \tag{5.8}$$

There is always a scale u_{UV} above which string theory is no longer weakly coupled. For this, we need a further restriction on N_c and λ:

$$\frac{u_{UV}}{u_0} \simeq \frac{N^{4/3}}{\lambda^2} \gg 1. \tag{5.9}$$

The low-energy theory on the D8-branes is the non-Abelian Dirac-Born-Infeld (DBI) action plus a Wess-Zumino term. Since the D8 and anti-D8 are continuously connected, we can write an action on a single extended stack of N_f D8-branes. We will mostly focus on the $N_f = 2$ case. The DBI action in the weak field limit is just the Yang-Mills action, so that

$$\begin{aligned} S = -k \int d^4x du \frac{u^{5/2}}{h(u)^{1/2}} \frac{1}{2} \mathrm{tr} \\ \times \left(\left(\frac{L}{u}\right)^3 \mathcal{F}_{\mu\nu}\mathcal{F}^{\mu\nu} + 2h(u)\mathcal{F}_{\mu u}\mathcal{F}^{\mu u} \right) \\ + \mathcal{O}(\mathcal{F}^4) + \frac{N_c}{24\pi^2} \int \omega_5^{N_f}(\mathcal{A}), \end{aligned} \tag{5.10}$$

where we raised indices with $\eta^{\Gamma\Delta}$, and the coefficient k is given by

$$k = \frac{L^{3/2}}{2^4 3\pi^4 g_s \alpha'^{5/2}}. \tag{5.11}$$

This can be written as a theory living on an effective 5D effective metric which takes into account the effect of the dilaton:

$$ds = \frac{u^2}{u_0^2} dx^2 + \frac{L^3}{u_0^2 u h(u)} du^2. \tag{5.12}$$

We can change variables from u to z with

$$1 + \frac{z^2}{z_0^2} = \frac{u^3}{u_0^3} \quad \text{with} \quad z_0^2 = \frac{4L^3}{9u_0} = R_5^2. \tag{5.13}$$

This brings the metric to the form (3.1), and the action (5.10) to (3.2) in the x^μ, z coordinates in units $z_0 = R_5 = 1$.

Figure 9 shows how the instanton bag solution is embedded in the D8's world volume. The terms (5.10) are a truncation of the DBI action to the first YM term. The original DBI action for the D8 brane is

$$S_{\mathrm{DBI}} = T_8 \int d^9x e^{-\phi} \mathrm{tr} \sqrt{-\det(g_{\Gamma\Delta} + 2\pi\alpha' \mathcal{F}_{\Gamma\Delta})}. \tag{5.14}$$

To check if the truncation of the DBI action to the YM term is a good approximation, we have to check if the three corrections

$$\frac{(\alpha' B)^2}{g_{11}g_{22}}, \qquad \frac{(\alpha' F_{3u})^2}{g_{33}g_{uu}}, \qquad \frac{(\alpha' \hat{F}_{u0})^2}{g_{00}g_{uu}} \tag{5.15}$$

are negligible for any u. In the almost-BPS limit, that is, $Q \ll \Lambda^2$, the first two in (5.15) are both of order 1. So, as it happens for an instanton in isolation, the YM term receives order 1 corrections from the higher derivative terms. This is mitigated by the fact that the self-dual solutions are also solutions of the DBI action in flat space [36]. Even in the large $Q \ll \Lambda^2$ limit, computed on the solution (4.29), these higher derivative corrections remain non-negligible.

In the effective metric (3.1) the full DBI plus Chern-Simons (CS) action is

$$\begin{aligned} \mathcal{S} = -\int d^4x dz C \mathrm{tr} \sqrt{-\det\left(g_{\Gamma\Delta} + \frac{2}{C^{1/2}}\mathcal{F}_{\Gamma\Delta}\right)} \\ + \frac{8}{3\Lambda} \int d^4x dz \omega_5(\mathcal{A}), \end{aligned} \tag{5.16}$$

where

$$C = \frac{\Lambda^2}{16(1+z^2)^{1/2}}, \tag{5.17}$$

and we used the same rescaling as (3.6). For the almost-BPS regime, from (4.1) and (4.8), the non-Abelian field is $B = \Lambda/\sqrt{6}$ inside the instanton bag. The correction from the higher derivative terms is thus of order $B/C^{1/2} = 4/\sqrt{6}$, which is indeed non-negligible and does not depend on Λ. A detailed study of the instanton bag solution using the full DBI + CS action is beyond the scope of this paper. We do not expect, at least in the almost-BPS regime, a qualitative change in the solution.

VI. CHIRAL SYMMETRY RESTORATION

The purpose of this section is to discuss the phenomenon of chiral symmetry restoration at high density.

Let us first discuss the basic features of chiral symmetry breaking in the SS model with the linear expansion in eigenmodes. The theory lives in the effective geometry (3.1), where the left and right flavor branes correspond to the left and right limits of the holographic coordinate $z \to \pm\infty$. The YM action in this metric is

$$S = \int d^4x dz \mathrm{tr}\left(-\frac{1}{2H(z)^{1/2}} {F_{\mu\nu}}^2 - H(z)^{3/2} {F_{\mu z}}^2 \right). \tag{6.1}$$

We linearly expand around the vacuum state

$$A_\mu = \sum_n B_\mu^n(x_\mu)\psi_n(z) \qquad A_z = \sum_n \varphi^n(x_\mu)\phi_n(z), \tag{6.2}$$

We take ϕ_n to be the derivative of ψ_n. The boundary conditions correspond to the vanishing of the sources at the conformal boundaries:

$$\psi_n(\pm\infty) = 0 \quad \text{for } n > 0. \tag{6.3}$$

This is the condition that quantizes the mesons states. n odd or even correspond, respectively, to even or odd states, and $n = 0$ is a case to be treated with special care. ψ_n solves the equation

$$H(z)^{1/2}\partial_z(H(z)^{3/2}\partial_z\psi^{\pm}_{(k)}(z)) + k_n^2\psi^{\pm}_{(k)}(z) = 0. \tag{6.4}$$

The action becomes then

$$S = \sum_n (\psi_n, \psi_n) \int d^4x \left(-\frac{1}{4}(\partial_\mu B^n_\nu - \partial_\nu B^n_\mu)^2 + \frac{k_n^2}{2}(B^n_\mu - \partial_\mu \varphi^n)^2 \right), \tag{6.5}$$

and the metric in $\psi(z)$ functional space is

$$(\psi_1, \psi_2) = \int dz H(z)^{-1/2}\psi_1(z)\psi_2(z), \tag{6.6}$$

with ψ_n, ψ_m that are orthogonal if $n \neq m$. For $n \geq 1$ we can eliminate φ's with a gauge transformation, and the action is then that of a vector boson with mass k_n. When $n = 0$, also $k_0 = 0$, and this gives the action of the pion. This is a special case because the boundary condition (6.3) is not satisfied, but nevertheless there is no source at the boundary.

If we expand around another state, we need the particular multi-instanton background which solves the finite density problem. The spectrum in the dual theory always consists in a tower of vector bosons plus the pions.

Vector mesons come in pairs, one vectorial V and one axial A, under the parity symmetry $z \to -z$. In our conventions, these correspond, respectively, to the choice of n being odd or even. One of the simplest observables that probes chiral symmetry breaking is the mass splitting between the axial and vectorial states:

$$\eta_m = \frac{M_{2m} - M_{2m-1}}{M_{2m} + M_{2m-1}}. \tag{6.7}$$

This test can be performed at every level $m > 0$, although the lower ones give, in general, the biggest η. If η_m is different from zero, chiral symmetry is broken. If η_m is zero, or almost zero, the V and A states are degenerate, and chiral symmetry is restored, or almost restored. In the vacuum, the two left and right branes are connected by the geometry, and chiral symmetry is thus broken. This may not be the case in the presence of something in the middle that could prevent communication between the two sides.

Chiral symmetry is restored, for example, at high temperature in the SS model. Introducing finite temperature leads to competition between the Euclidean time circle τ and the x_5 circle on which to close the topology. This may lead to a phase transition with chiral symmetry restored. In this case, the geometry of space-time has a Hawking-Page phase transition, and the two branes become disconnected by the presence of a horizon. This is a drastic change in the topology, and the V and A states become absolutely degenerate; i.e., η_m is exactly zero for every level m. At finite chemical potential, the situation is more subtle. We will be mainly interested in the zero temperature case, so the topology of space-time remains unchanged (3.1). Chiral symmetry restoration can be explained just within the effective action (3.2).

We consider first a toy model that illustrates a simplified version of the phenomenon we want to discuss. This is the quantum mechanical problem of a particle in a double-well potential with Hamiltonian

$$H = -\frac{1}{2}\left(\frac{d}{dx}\right)^2 + \frac{v^2}{2}(x^2 - 1)^2. \tag{6.8}$$

The potential has a parity symmetry $x \to -x$. In case of a very large potential barrier, $v \gg 1$, we can approximate the eigenstate energies as

$$E_{m,\pm} \simeq \frac{1}{2} + m \mp \mathcal{O}(e^{-4v/3}) \quad \text{for } m \ll v, \tag{6.9}$$

with $m \in \mathbb{N}$. These states are localized near the two vacua of the potential and come in pairs. The potential provides a barrier for the states that have energy below its maximum height. For the states below this barrier, we have an approximate degeneracy between V and A states. The splitting between odd and even states can occur only through the tunneling below the barrier, and it is thus suppressed exponentially by the instanton action $e^{-4v/3}$. The situation in HQCD at high density, as we are going to see, is analogue to this toy model. The instanton charge provides a potential barrier between the left and right boundaries. We then have to determine under which conditions the barrier can seal the two sides from communication with each other, at least for some of the low-energy states, thus providing a mechanism for an effective chiral symmetry restoration. Note that, as for the toy model, the chiral symmetry restoration can never be exact but only up to exponentially small terms. This is expected because, unlike the high temperature case, the left and right branes are always connected by the geometry.

We now consider a second toy model, which is a step closer to the real thing. We take a charged particle living on a strip $-L < z < L$ and $-\infty < x < \infty$ and coupled to a background gauge field. The equation of motion is the following covariant version of the Klein-Gordon equation:

$$\left(\frac{1}{2}(\partial_t - iA_t)^2 - \frac{1}{2}(\partial_x - iA_x)^2 - \frac{1}{2}(\partial_z - iA_z)^2\right) \times \psi(t, x, z) = 0. \tag{6.10}$$

In a static background, we can solve the eigenvalues equation

$$\left(-\frac{1}{2}(\partial_x - iA_x)^2 - \frac{1}{2}(\partial_z - iA_z)^2\right)\psi_n(x,z) = \epsilon_n \psi_n(x,z). \tag{6.11}$$

This is the same as the Schrödinger equation for a nonrelativistic quantum particle with mass$/\hbar^2 = 1$. This analogy may be useful. For states which do not have momentum in the x direction, the eigenvalues λ_n are related to the mass in the holographic interpretation, precisely

$$\epsilon_n = \frac{M_n^2}{2} \quad \text{for } k_x = 0. \tag{6.12}$$

In the vacuum $A_{x,z} = 0$, the spectrum of the operator (6.11) is $\epsilon_n = (1+n)^2/L$, where n being odd or even corresponds to the parity with respect to $z \to -z$ and clearly there is no degeneracy between V and A states. We then turn on a constant magnetic field $F_{xz} = F$ in a smaller strip $-z_* < z < z_*$ with $z_* < L$. The phenomenon of magnetic trapping is quite clear by considering the classical particle trajectories in Fig. 10. This in the sense of the nonrelativistic analogy mentioned before. For a particle to be able to cross the magnetic strip, the radius of the trajectory in the constant magnetic field zone $\sqrt{2\epsilon}/F$ must be at least equal to the strip size $2z_*$. There is an effective energy barrier $\simeq (Fz_*)^2$ between the left and right regions. The left and right states, if confined in the regions without the magnetic field, have energies

$$\epsilon_{m;\mathrm{V,A}} = \frac{\pi^2(1+m)^2}{2(L-z_*)^2} \mp \mathcal{O}(e^{-\alpha F z_*^2}) \tag{6.13}$$

with $m \in \mathbb{N}$:

$$l_p \simeq \frac{1+m}{(L-z_*)F}. \tag{6.14}$$

The condition to have V and A degeneracy is $l_p \ll z_*$, which, for the lowest state $m = 0$, is

$$\frac{1}{(L-z_*)F} \ll z_*. \tag{6.15}$$

To be more explicit, we take the following gauge to reproduce the desired magnetic field,

$$\begin{aligned} A_x &= 0 && z_* \geq z \geq L \\ A_x &= F(z - z_*) && -z_* \leq z \leq z_* \\ A_x &= -2Fz_* && -L \geq z \leq -z_*, \end{aligned} \tag{6.16}$$

with $A_t = A_z = 0$. The eigenstates can be written as

$$\psi(t,x,z) = e^{ik_t t - ik_x x}\psi_n(z), \tag{6.17}$$

where $k_t^2 - k_x^2 = M_n^2$ is the mass square from the x,t perspective. With this ansatz, the eigenvalue equation becomes

$$-\frac{1}{2}\psi_n(z)'' + \frac{(F(z-z_*) - k_x)^2}{2}\psi_n(z) = \frac{M_n^2}{2}\psi_n(z), \tag{6.18}$$

which is the analogue of (6.4). The wave function $\psi_n(z)$ is exponentially suppressed in the magnetic field region. This damping is smaller if we increase the particle mass M_n and/or if we give a momentum in the x direction, as is also clear from Fig. 10. For the low-energy states, the penetration length is given by formula (6.14).

We now consider a third toy model (Fig. 11), which contains yet another different effect that will have to be considered when we will deal with the real thing. We take the same charged particle as before, living on a strip $-L < z < L$ and $-\infty < x < \infty$ and coupled to a background gauge field. We then turn on a pure gauge field $A_x = C$, with C a constant in a smaller strip $-z_* < z < z_*$, with $z_* < L$:

$$\begin{aligned} A_x &= 0 && z_* + \delta \geq z \geq L \\ A_x &= C && -z_* \leq z \leq z_* \\ A_x &= 0 && -L \geq z \leq -z_* - \delta, \end{aligned} \tag{6.19}$$

with $A_t = A_z = 0$. The two walls at the edges of the strip have thickness $\delta \ll z_*$. Here a magnetic field F_{xz} is inevitably turned on to have the matching of the gauge field. We assume that this happens in the simplest way, a linear function homogeneous in x. So the magnetic field inside the two walls is, respectively, $F_{xz} = \pm C/\delta$.

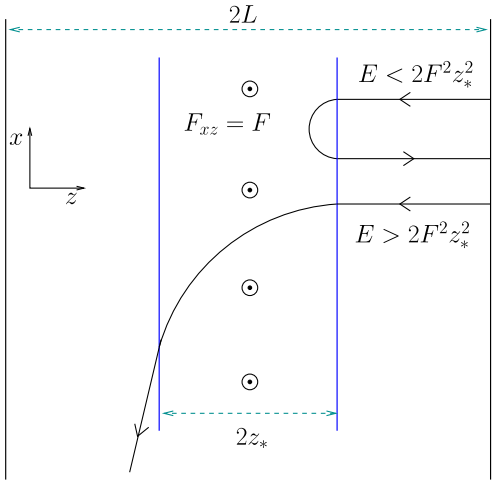

FIG. 10 (color online). Charged particle tunneling a magnetic field strip.

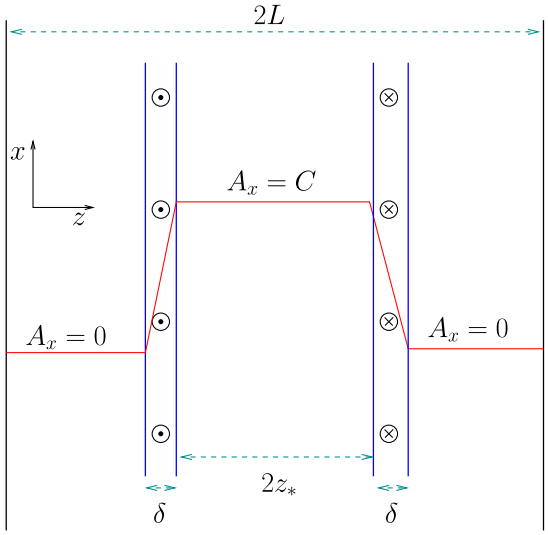

FIG. 11 (color online). Charged particle tunneling a "pure gauge" strip.

There is now a massless eigenstate that can propagate inside the strip since it is a pure gauge. The only difference is that this state must have a phase changing in the x direction to cancel the constant field e^{iCx}. So the main source of tunneling between the left and right side takes place inside the two walls of thickness δ, and is just given by the overlap between the massless states inside and outside the strip. The penetration length is now given by

$$l_p \simeq \frac{(1+m)\delta}{(L-z_*)C}. \tag{6.20}$$

The condition to have V and A degeneracy is $l_p \ll \delta$, which, for the lowest state $m = 0$, is

$$\frac{1}{(L-z_*)C} \ll 1. \tag{6.21}$$

Note that δ disappears from this condition.

Now we finally consider the real problem of HQCD in the instanton bag background. The problem is quite complex, and we cannot provide an analytic solution for the wave functions and the spectra as in the the vacuum state (6.4). We have to rely on analogies with the previous toy models. There are two different sources of tunneling we need to consider: one is mimicked by the second toy model of Fig. 10, and the other by the third toy model of Fig. 11.

The theory is defined on the metric (3.1), which is effectively a box with finite size, and this is what provides the quantization of the vector mesons' masses. The analogy with the previous two toy models is that the size of the strip L is the curvature scale.

We begin from the almost-BPS limit, which is valid in the region of densities $\Lambda^{3/2} \ll Q \ll \Lambda^2$. The $\Lambda^{3/2}$ lower bound is when the instantons begin to populate the holographic direction, and it also coincides with the microscopic wall structure, $l \simeq \delta \simeq 1/\sqrt{\Lambda}$, being smaller than the distance between the two walls, which is of order Q/Λ^2. The upper bound coincides with the wall position being much smaller than the curvature scale $z_w \simeq Q/\Lambda^2 \ll 1$. In this case, the wavelength of the particle confined in the empty sides is of order 1 [this is the analogue of $1/(L-z_*)$ in the toy model].

The first effect to consider is the tunneling as in Fig. 10. Between the two walls the fields are

$$F_{12} = F_{3z} = BU(x_1,x_2)t_{\mathrm{su}(2)}U(x_1,x_2)^{-1}. \tag{6.22}$$

A gauge transformation $U(x_1,x_2)$ is necessary, as we discussed in Sec. II, for the gauge fields not to have Dirac string singularities at both boundaries. The magnetic fields oscillate in all the su(2) generators. The vector boson states are instead waves coming from the empty sides in a fixed generator of the su(2) algebra.

The F field of the toy model in Fig. 10 is the analogue of this F_{zx_3} field. We will neglect the magnetic field F_{12} for simplicity. First, we check if the oscillations of the magnetic field generator are fast enough with respect to the momentum of the wave hitting the monopole wall from the empty side. This is indeed the case because the momenta of the waves confined in the empty regions are of order 1 while the momentum of the monopole wall lattice is $1/l \simeq 1/\sqrt{\Lambda}$. The vector boson states do not have enough energy to resolve the microscopic structure of the wall or to see the fluctuations of the magnetic fields (6.22). Then we have to check if the size of the magnetic strip is large enough to separate the left and right sides. The penetration length is of order $1/F \simeq 1/\Lambda$ and is much smaller than the wall's distance $z_w \simeq Q/\Lambda^2$ in this regime. Therefore, the two sides are indeed separated by a potential barrier, at least for the channel described by Fig. 10.

There is yet another possible source of tunneling. The monopole wall solution is essentially an Abelian solution far from the wall. In the Dirac gauge, the fields are all directed in one particular direction in the algebra su(2); see (2.3), (2.4). So the states of the vector boson fields which are directed in the same direction are completely transparent to the magnetic fields and they pass through the region between the two walls as free fields. The hedgehog gauge does not make these massless states disappear; they just have particular winding in the x_1 and x_2 direction to compensate for the gauge transformation. This is an exact analogue to what happens in the toy model of Fig. 11. The condition for having a barrier is that the wavelength of the particle confined in the empty sides must be much smaller that the microscopic wavelength $1/l$, and this we already checked to be the case.

We then go to the high-density limit $Q \gg \Lambda^2$, and we have to compute the equivalent of the energy scale (6.13) in the toy model. For this, it is convenient to go first in the η

coordinate where the metric is conformally flat, which for $z \gg 1$ and $\eta \ll 1$ is

$$ds^2 = z(\eta)^{4/3}(dx_\mu dx^\mu + d\eta^2) \qquad z(\eta) \simeq \frac{27}{\eta^3}. \tag{6.23}$$

The typical momentum of a particle confined in the empty region $z > z_W$, in these coordinates, is

$$k_\eta \simeq \frac{1}{\eta_w} \simeq \frac{3}{z_w^{1/3}}. \tag{6.24}$$

We then use the coordinate transformations to go in the $\tilde{x}, \tilde{z}$ coordinates, the ones in which the metric is (4.35) near the wall. The result is

$$k_{\tilde{z}} \simeq \frac{k_\eta}{z_w^{2/3}} \simeq \frac{3}{z_w}. \tag{6.25}$$

This is the momentum of the wave hitting the monopole wall in a locally Minkowski frame.

The next step is to compare this with the lattice size of the monopole wall. The following inequalities,

$$k_{\tilde{z}} \ll \frac{1}{l} \Rightarrow \Lambda^{1/2} \ll Q^{1/2}, \tag{6.26}$$

mean that the momentum $k_{\tilde{z}}$ is never large enough to see the microscopic structure of the wall, so we can average out the fluctuations of the magnetic field. Then we want to estimate the penetration length of the wave with momentum (6.25) when it enters the magnetic field region. The penetration length is from the equation

$$l_p \simeq \frac{k_{\tilde{z}}}{F_{\tilde{3}\tilde{z}}} \propto \frac{1}{Q^{2/5}\Lambda^{1/5}}, \tag{6.27}$$

which is even smaller than the wall thickness δ. Thus, the two sides are not communicating also in the $Q \gg \Lambda^2$ limit.

With the chiral symmetry restoration being only up to exponentially small terms, the V-A mass splitting is never exactly zero, and in particular the pion, as a massless state in the spectrum of the theory, is always present. Testing chiral symmetry restoration with the pion would be more complicated than just computing the spectrum; it would require us to check the pion self-interaction or the pion vector meson interaction. The pion wave function $\phi_0(z)$ is approximately constant in the two empty sides of the instanton bag, with opposite sign, and joined by an exponentially suppressed tail in the middle. This implies that the higher derivative interactions between pions and between pions and the massive vector bosons should be exponentially suppressed. It would be interesting to understand this aspect in terms of the chiral condensate, as in [37,38].

VII. CONCLUSIONS

In the first part of the paper, we discussed a multi-instanton solution in flat space which is periodic in three directions and finite in the fourth direction. We called this an instanton bag because, in some opportune limit, it can be described by a homogeneous distribution of self-dual fields trapped between a monopole wall and a Kaluza-Klein monopole wall. We embedded the instanton bag in the Sakai-Sugimoto model. This is the dual of a phase of high-density baryons in the QCD-like theory defined on the boundary. The parameters of the solutions have been determined by the constrained energy minimization, analytically solved in two limits of intermediate and large densities, and confronted with the numerical solution.

A transition from a lattice of instantons and a lattice of monopoles and KK monopole pairs has been discussed in [11] under the name of "dyonic salt." Our construction is somehow an extension of this because we show, using the monopole walls, how to extend this to higher densities where the holographic direction is also probed. The fact that at high densities the instantons start to probe the holographic direction has been discussed [7,9,10] and linked to the existence of a quarkyonic phase. We showed that a configuration similar to the dyonic salt can be extended to arbitrarily high densities and probe the holographic direction.

We still cannot perform the minimization over all the possible multi-instanton moduli space. The instanton bag configuration we considered in this paper is just one particular case, for we can compute the fields and the energy and then minimize the moduli.

This instanton bag phase is intrinsically nondilute; i.e., the individual instantons' components cannot be distinguished and are larger than their average separation. Previous results in the toy model [1] and also the qualitative analysis of Sec. III showed that nondilution is an inevitable feature of large density solutions and becomes applicable exactly when the solitons start to populate the holographic direction.

The restoration of chiral symmetry is related to the nondilution of this phase. The non-Abelian field strength is continuously spread in the bulk, as opposed to a dilute phase in which it is confined to the instanton cores. This considerably affects the equation of motion for the gauge fields in the bulk, and thus creates a barrier between the left and right branes, leading to an effective chiral symmetry restoration.

ACKNOWLEDGMENTS

I thank D. Tong, M. Blake, and K. Wong for discussions and collaboration to the initial stage of this project. I thank P. Sutcliffe for discussions, in particular during the closely related projects [1,29]. This work was partially funded by the EPSRC Grant No. EP/K003453/1 and now by the grant "Rientro dei Cervelli, RLM" of the Italian government.

[1] S. Bolognesi and P. Sutcliffe, J. Phys. A **47**, 135401 (2014).
[2] S. Bolognesi, Nucl. Phys. **B752**, 93 (2006).
[3] P. Sutcliffe, Phys. Rev. D **85**, 125015 (2012).
[4] D. Harland, S. Palmer, and C. Saemann, J. High Energy Phys. 10 (2012) 167.
[5] D. V. Deryagin, D. Y. Grigoriev, and V. A. Rubakov, Int. J. Mod. Phys. A **07**, 659 (1992).
[6] E. Shuster and D. T. Son, Nucl. Phys. **B573**, 434 (2000).
[7] J. de Boer, B. D. Chowdhury, M. P. Heller, and J. Jankowski, Phys. Rev. D **87**, 066009 (2013).
[8] L. McLerran and R. D. Pisarski, Nucl. Phys. **A796**, 83 (2007).
[9] V. Kaplunovsky, D. Melnikov, and J. Sonnenschein, J. High Energy Phys. 11 (2012) 047.
[10] V. Kaplunovsky and J. Sonnenschein, J. High Energy Phys. 04 (2014) 022.
[11] M. Rho, S.-J. Sin, and I. Zahed, Phys. Lett. B **689**, 23 (2010).
[12] Y.-L. Ma, M. Harada, H. K. Lee, Y. Oh, B.-Y. Park, and M. Rho, Phys. Rev. D **88**, 014016 (2013).
[13] M. Rozali, H.-H. Shieh, M. Van Raamsdonk, and J. Wu, J. High Energy Phys. 01 (2008) 053.
[14] K.-M. Lee, Phys. Lett. B **445**, 387 (1999).
[15] R. S. Ward, Phys. Rev. D **75**, 021701 (2007).
[16] S. Bolognesi and D. Tong, J. High Energy Phys. 01 (2011) 153.
[17] P. Sutcliffe, J. High Energy Phys. 08 (2011) 032.
[18] S. A. Cherkis and R. S. Ward, J. High Energy Phys. 05 (2012) 090.
[19] M. Hamanaka, H. Kanno, and D. Muranaka, Phys. Rev. D **89**, 065033 (2014).
[20] S. A. Cherkis, J. High Energy Phys. 06 (2014) 027.
[21] R. Maldonado and R. S. Ward, Phys. Lett. B **734**, 328 (2014).
[22] E. J. Weinberg and A. H. Guth, Phys. Rev. D **14**, 1660 (1976).
[23] K.-M. Lee and P. Yi, Phys. Rev. D **56**, 3711 (1997).
[24] K.-M. Lee and C.-h. Lu, Phys. Rev. D **58**, 025011 (1998).
[25] T. C. Kraan and P. van Baal, Nucl. Phys. **B533**, 627 (1998).
[26] K. Lee (private comunication).
[27] D. K. Hong, M. Rho, H.-U. Yee, and P. Yi, Phys. Rev. D **76**, 061901 (2007).
[28] H. Hata, T. Sakai, S. Sugimoto, and S. Yamato, Prog. Theor. Phys. **117**, 1157 (2007).
[29] S. Bolognesi and P. Sutcliffe, J. High Energy Phys. 01 (2014) 078.
[30] D. K. Hong, arXiv:1409.8139.
[31] Y. Kim, S. Lee, and P. Yi, J. High Energy Phys. 04 (2009) 086.
[32] K. Ghoroku, K. Kubo, M. Tachibana, T. Taminato, and F. Toyoda, Phys. Rev. D **87**, 066006 (2013).
[33] C. Ford, J. M. Pawlowski, T. Tok, and A. Wipf, Nucl. Phys. **B596**, 387 (2001).
[34] T. Sakai and S. Sugimoto, Prog. Theor. Phys. **113**, 843 (2005).
[35] E. Witten, Adv. Theor. Math. Phys. **2**, 505 (1998).
[36] V. Kaplunovsky and J. Sonnenschein, J. High Energy Phys. 05 (2011) 058.
[37] O. Aharony and D. Kutasov, Phys. Rev. D **78**, 026005 (2008).
[38] S. Seki and S.-J. Sin, J. High Energy Phys. 08 (2012) 009.